# Lensing system and Fourier transformation using epsilon-near-zero metamaterials

M. Navarro-Cía,[1,2,3,*] M. Beruete,[2,†] M. Sorolla,[2,‡] and N. Engheta[3,§]

[1]*Experimental Solid State Group, Department of Physics, Imperial College London, London SW7 2AZ, United Kingdom*

[2]*Millimeter and Terahertz Waves Laboratory, Universidad Pública de Navarra, E-31006 Pamplona, Spain*

[3]*Department of Electrical and Systems Engineering, University of Pennsylvania, 200 South 33rd Street, ESE 203 Moore, Philadelphia, Pennsylvania 19104, USA*

(Received 22 November 2011; revised manuscript received 23 September 2012; published 23 October 2012)

Metamaterials and metastructures with effective relative permittivity near zero exhibit unusual wave properties such as uniform phase distributions across such domains. Here we discuss the possibility of using $\varepsilon$-near-zero (ENZ) metamaterials for lensing and Fourier transforming. Owing to the possibility of having ENZ metamaterials in different wavelength regimes, the concepts shown here can be utilized at any frequency bands in which such materials can be constructed.

DOI: 10.1103/PhysRevB.86.165130 PACS number(s): 81.05.Xj, 42.30.Kq, 42.79.Bh, 78.67.Pt

Extreme-parameters metamaterials,[1–6] especially $\varepsilon$-near-zero (ENZ) metamaterials, have attracted a great deal of attention in recent years. Unlike other metamaterials possessing negative constitutive parameters that usually happen near resonances, the ENZ properties are displayed somewhat away from resonances, where losses are less.[7] The ENZ regime may be obtained just slightly above the plasma frequency of materials, for example, above plasma frequency in metal and highly doped semiconductor at optics and THz, respectively. At lower frequencies, a simple yet effective approach is based on arrangements of hollow waveguides at cutoff frequencies.[4,8] Some of the exciting features of ENZ metamaterials include the phenomenon of supercoupling, optical lumped insulator elements, and substrates for the optical displacement-current wires in metatronics.[2–4,8] The ENZ metamaterials have played roles in tunneling, beam forming, energy squeezing, sensing, and cloaking.[4–6,8–12]

Fourier transforms are ubiquitous in modern society due to its broad utility in many branches of science and engineering, such as signal processing, antennas, imaging (e.g., magnetic resonance imaging, x rays, tomography, radar, etc.), holography, spatial distribution and spectral composition of radiation sources, and spectroscopy, just to name a few.[13,14] The propagation and diffraction of electromagnetic waves may provide Fourier transformation. It is well known that a Fraunhofer diffraction pattern is directly related to the Fourier transform of the source distribution.[15] However, the distances involving far-zone patterns are not usually practical, and instead converging lenses have solved this problem. It has been demonstrated decades ago that lenses bring the Fraunhofer diffraction pattern to its focal length, significantly reducing the space required for this spatial Fourier transform.[13,14]

In this paper we numerically demonstrate that anisotropic ENZ metamaterials and ENZ metastructures may hold the promise for the design of novel lensing systems and consequently Fourier transforming, expanding thus the range of potential applications of these specialized media. First, we consider a homogeneous isotropic ENZ material as a starting point. In the next stage we provide a thorough numerical analysis of a real implementation of the Fourier transform system. Finally, using the numerical simulation, the proposed anisotropic metastructure is compared with the structure with homogeneous isotropic ENZ materials. For simplicity we reduce all analyses to two dimensional with transverse-magnetic (TM) excitation. Numerical simulations have been conducted using the finite-integration-technique software CST Microwave Studio™.[16]

Let us assume a homogenous isotropic material whose relative permittivity is near zero. The profile of a lens made of such ENZ material, which should be designed to perform the Fourier transform may be a plano-concave shape [Fig. 1(a), assuming without loss of generality that the input face is planar and the output face is a concave circular arc]. This is due to the fact that the phase front at the exit face of an ENZ material conforms to the shape of the exit face.[5] This can also be easily explained using geometrical optics.[17] Let us consider the effect of the plano-concave lens on a normally incident unit-amplitude (1 V/m) plane wave impinging on its planar input face. If the lens indeed operated as a Fourier transformer, one would expect a sinc function at its focal length rather than a $\delta$ function since the finite size of the lens' front face limits the spatial range of the incident signal. This is mathematically represented as follows[13]:

$$U_{z_f}(x) = \frac{\exp\left(i\frac{k}{2z_f}x^2\right)}{i\lambda_0 z_f}\int_{-\infty}^{\infty} A(u)\exp\left(-i\frac{2\pi}{\lambda_0 z_f}xu\right)du = \frac{\exp\left(i\frac{k}{2z_f}x^2\right)}{i\lambda_0 z_f}\mathscr{F}[A(u)] \propto \operatorname{sinc}\left(\frac{x}{\lambda_0 z_f}l\right), \quad (1)$$

where $U_{z_f}(x)$ is the complex field distribution at the back focal plane, $A(u)$ is a rectangular function that accounts for the finite dimensions of the lens and is 1 within the limits of the lens (from $-l/2$ to $l/2$) and 0 outside, $z_f$ is the focal length, $k$ is the wave vector, $\lambda_0$ is the free-space wavelength, $\mathscr{F}[A(u)]$ denotes the Fourier transform of $A(u)$, and the $\exp(-i\omega t)$ time-harmonic convention has been used.

Figure 1(b) shows the simulation results for the magnetic field distribution for the lens of radius $r = 5.1\lambda_0$ and width $l = 11\lambda_0$ (to avoid sharp edges) and made of an ENZ material (which for now has also permeability near zero in order to have the lens impedance matched to the free space, i.e., no reflection). For the material dispersion, a Drude model has been chosen for both permittivity and permeability with $\varepsilon_\infty = \mu_\infty = 1$, plasma frequency $\omega_p = 3.76991 \times 10^{11}$ rad/s

 

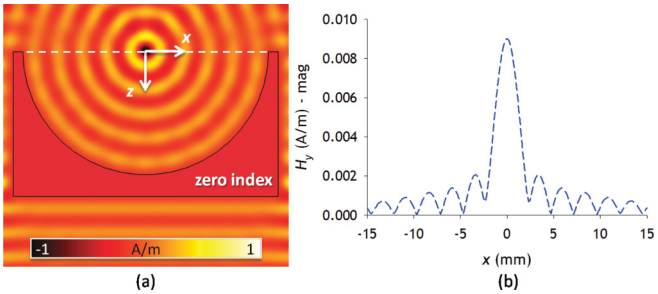


FIG. 1. (Color online) (a) and (b) Simulation results for the magnetic field distribution (snap shot in time) $H_y$ in a plano-concave lens formed by an isotropic homogeneous $\varepsilon = \mu = 0$ material, illuminated by a normally incident unit-amplitude plane wave with the TM polarization: (a) top view, $x$-$z$-plane; (b) along the focal plane, $x$ direction. The white dashed line in (a) shows the cross section corresponding to (b).

(60 GHz), and collision frequency $\nu_c = 3.76991 \times 10^9$ Hz. A mesh cell resolution of 0.28 mm × 0.28 mm × 0.28 mm has been chosen to map accurately the geometry. In addition to its focusing effect exhibiting a depth of focus (i.e., distance between the longitudinal axial −3 dB points) along $z$ of 5.2 mm, the lens clearly generates a sinc-like function at its back focal plane. The quantitative comparison of this result (as well as the practical consideration subsequently proposed) with the theoretical results expected from an ideal Fourier transformer is left for later discussion.

For implementation of such ENZ Fourier transform operator we exploit here the concept of waveguides near cutoff with extremely small height but suitable width to allow performance near cutoff (the filling factor of the unit cell, i.e., the ratio of the volume of hollow waveguide to the volume of the unit cell, is very small).[4–6,8] This effective anisotropic homogeneous ENZ medium can be described by a lossless Drude-type model for the transverse components of permittivity tensor $\varepsilon_{xx\_\mathrm{eff}}$ and $\varepsilon_{yy\_\mathrm{eff}}$, whereas $\varepsilon_{zz\_\mathrm{eff}} = -\infty$ since for the plane wave eigenstate with the electric field along the $z$ axis, no propagation in such effective medium with the wave vector in the $x$-$y$ plane is present[18]:

$$\bar{\bar{\varepsilon}}_{\mathrm{eff}} = \begin{pmatrix} \varepsilon_{xx\_\mathrm{eff}} & 0 & 0 \\ 0 & \varepsilon_{yy\_\mathrm{eff}} & 0 \\ 0 & 0 & \varepsilon_{zz\_\mathrm{eff}} \end{pmatrix} = \begin{pmatrix} 1 - \left(\frac{c\pi}{h_y \omega}\right)^2 & 0 & 0 \\ 0 & 1 - \left(\frac{c\pi}{h_x \omega}\right)^2 & 0 \\ 0 & 0 & -\infty \end{pmatrix}, \quad (2)$$

where $h_x$ and $h_y$ are the height and width of the waveguide, respectively, and $\omega$ is the angular frequency.

Figure 2(a) shows the sketch of such proposed implementation. A unit cell is shown in which a narrow hollow waveguide designed to be operating near its cutoff frequency may be carved. The waveguide is ultranarrow and its volume occupies a very small volume fraction. The theoretical formalism presented in Ref. 19 provides the foundation behind this particular condition, namely, the impedance mismatch arisen from the ENZ structure (i.e., the transverse impedance of the waveguide near cutoff) can be reduced by the choice of very small volume fraction. As a rule of thumb, $h_y \approx \lambda_0/2$ and $d_x = 10h_x$ are chosen to optimize transmission and reduce reflection.[20] In particular, the dimensions of our design are $h_y = 2.5$ mm, $d_y = 3$ mm, $h_x = 0.1$ mm, $d_x = 1$ mm, the radius of the lens $r = 25.5$ mm, the length of the central waveguide is 4.5 mm, and the total lens width is 51 mm. With these dimensions and TM illumination the frequency of operation falls within the $V$ band of the millimeter-wave regime, that is, 60.4 GHz, although there is no restriction to work at any other frequency range, as long as we can design the waveguide at cutoff. The design shown in Fig. 2 resembles the classical and metamaterial metallic lenses.[10,21–25] However, it must be noted that the underlying physics is completely different. The waveguides suggested here have a very small volume fraction in a unit cell, and owing to the fact that they are designed to operate near the cutoff frequency, they behave as an ENZ structure and therefore the phase distribution within each waveguide is indeed nearly uniform. This leads to the requirement of having a circular profile at its exit face in order to provide focusing effect at the back focal plane, but more importantly it removes the need for any Fresnel zoning technique (in the Fresnel lens, one removes the parts of material where the phase variation is a multiple of $2\pi$, resulting in a sawtoothlike profile). However, such sawtooth profile is not needed here, therefore reducing any significant penalty in the performance.[21] Moreover, unlike dielectric lenses, the above proposed metallic lenses using the waveguide at cutoff may perform a discrete Fourier transform. Nevertheless, by choosing $h_x \ll \lambda_0$, as is the case in our design in Fig. 2, this ENZ lens may indeed sample the incoming wave as many points in a wavelength, such effectively behaving in the domain of effective medium theory. It should also be mentioned that such a dense arrangement of waveguides viewed as a grating would not lead to major diffraction of the grating lobes, since the waveguide separation is far shorter than the operating wavelength.

Figure 2 shows the simulation results for the magnetic field distribution in the $x$-$z$ plane [Fig. 2(b)], electric and magnetic field distributions along the optical axis $z$ [Fig. 2(c)], and the magnetic field distribution at the focal plane along $x$ axis [Fig. 2(d)]. For these numerical calculations, a nonuniform grid has been used to discretize densely the hollow waveguide. The default cubic grid was set to 0.05 mm × 0.4 mm × 0.4 mm, and the hollow waveguides have been mapped with a mesh cell resolution up to 0.02 mm × 0.2 mm × 0.2 mm. In addition, for the sake of comparison in Figs. 2(c) and 2(d) the corresponding results for a homogeneous isotropic ($\varepsilon = 0$ and $\mu = 0$) lens (dashed lines), as well as the theoretical results for the expected Fourier transform [dark blue crosses in Fig. 2(d)] are shown. We note that the Talbot interference pattern[13] resulting from the periodicity is not seen at the output of this ENZ lens. This is due to the fact that the periodicity of unit cells is much smaller than the wavelength falling beyond the validity of Talbot, which relies on the smallness of the nonparaxiality parameter $\lambda_0/d_x$. Therefore, this ENZ lens is indeed seen by the input signal as an equivalent homogeneous ENZ medium rather than a grating. From Fig. 2 one can also notice the following features: (i) 21-fold enhancement of the electric field (with respect to the value of the incident electric field), (ii)

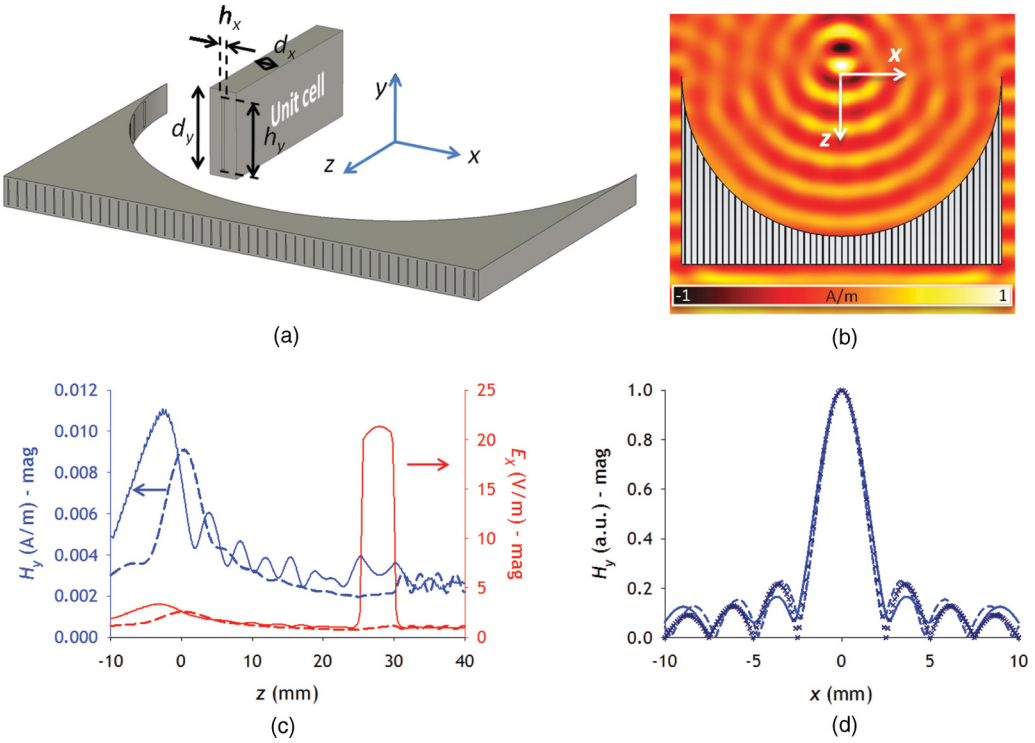


FIG. 2. (Color online) (a) Sketch of the proposed $\varepsilon$-near-zero metamaterial lens formed by an array of waveguide operating near their cutoff frequencies. Inset: Unit cell shown with its dimensions. (b) Simulation results for the magnetic field distribution $H_y$ along the $x$-$z$ plane. (c) $H_y$ (blue) and electric field distribution $E_x$ (red) along $z$ for the isotropic homogeneous zero-index lens (dashed lines) and the array of waveguides at cutoff (solid lines). (d) $H_y$ along the focal plane, $x$ direction: Solid blue lines correspond to the case of array of waveguides at cutoff, and dashed blue lines to the case of the isotropic homogeneous zero-index lens of Fig. 1, and dark blue crosses to the theoretical calculation of Fourier transform.

"static-like" response inside the lens volume in agreement with the ENZ characteristics[4–6,19,20]; and (iii) three sets of results at the focal plane, that is, expected theoretical Fourier transform, results from the homogeneous ENZ case, and the simulation results from the lens formed by an array of waveguides near cut off, all are compared with good agreement. The focal point does not appear exactly at $z = 0$ as consequence of the nonzero $\varepsilon$ of the ENZ lens and it is in good agreement with theoretical thin lens calculations: The focal length obtained from our numerical calculations is 28.78 mm, whereas the focal length of a thin lens with dielectric constant $\varepsilon = \varepsilon_{xx\_\mathrm{eff}}$ (60.4 GHz) is 28.81 mm.

The slight disparity between the results of the waveguide case and the other two sets may be arguably attributed to the edge effects and the small (though not totally negligible) angle and length dependence of the frequency at which the total transmission occurs. To give further insight on the latter issue, in Fig. 3 the resonance frequency at which the total transmission occurs for an infinite array as a function of angle of incidence (owing to the reciprocity, also angle of emergence) and waveguide length (i.e., array thickness) is plotted. As expected for long waveguides, the transmission happens at lower frequencies, approaching the ideal case of $\varepsilon_{xx\_\mathrm{eff}} = 0$ at 60 GHz, whereas for short waveguides the resonance frequency deviates from this theoretical value. This deviation can be explained by the coupling through the waveguide of reactive energy associated with the higher-order evanescent modes that are excited at the air-waveguide interfaces. Obviously for long waveguides, the coupling is reduced (the higher-order modes are evanescent inside) and the agreement with the theoretical frequency is more accurate. The proposed ENZ lens, however, does not suffer significant degradation in its performance despite this dispersion, because the redshift of the ENZ total transmission frequency expected when the waveguide length is increased as we move away from the center of the lens is compensated by the blue shift arisen from the increasing angle of emergence. Quantitatively, it is shown by the white symbols in Fig. 3 that each waveguide would need to work at different frequencies within the range from 60.18 to 60.42 GHz in order to ideally redirect all together the rays to the numerically computed focal point. This means that for a certain frequency, for instance our chosen 60.4 GHz, the lateral waveguides are not operating at their ideal total transmission point (and thus, free-space matched situation) but slightly offset. This is the origin of the increasing, yet small, reflections toward the sides of the lens at the input and output of the lens, see Fig. 2(b).

Now that we have shown the Fourier transformation of the truncated uniform input using the design in Fig. 2(a), we show how some other properties of Fourier transformation can be explored by this lens. Let us consider an obliquely incident plane wave impinging on the ENZ lens of Fig. 2(a). Mathematically, this can be represented as a constant function with a certain phase variation afforded by the pupil function of

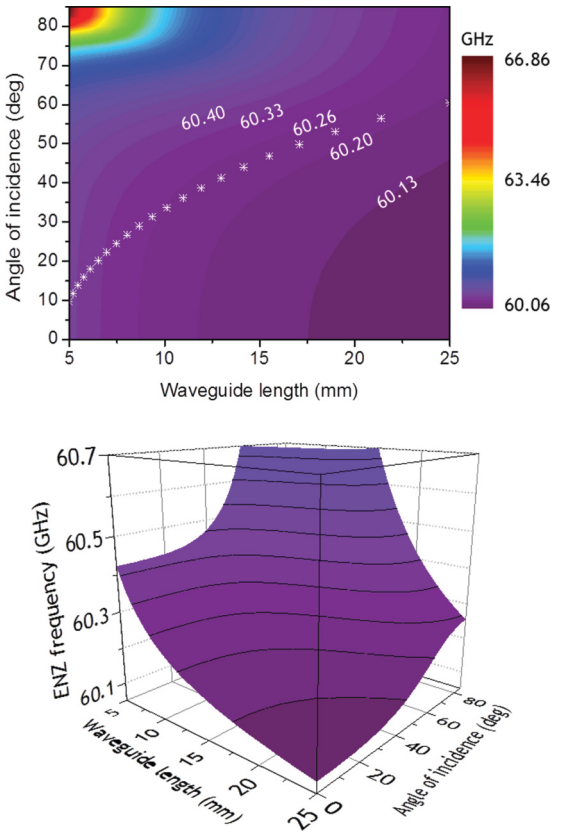


FIG. 3. (Color online) (Top) ENZ resonance frequency as a function of the waveguide length and the angle of incidence of a plane wave with TM polarization. The white symbols represent the desired angle of emergence for each waveguide of the ENZ lens when the focal length is the numerically found 28.78 mm. (Bottom) Zoom-in to the lowest frequency range.

the lens (i.e., a rectangle function). According to the translation property of Fourier transform, the function at the back focal plane must be again a sinc function but shifted away from the optical axis as follows[13]:

$$U_{z_f}(x) = \frac{\exp\left(i\frac{k}{2z_f}x^2\right)}{i\lambda_0 z_f}\int_{-\infty}^{\infty} A(u)\exp\left(-i\frac{2\pi}{\lambda_0}u\sin\theta\right) \times \exp\left(-i\frac{2\pi}{\lambda_0 z_f}xu\right)du$$
$$= \frac{\exp\left(i\frac{k}{2z_f}x^2\right)}{i\lambda_0 z_f}\mathscr{F}\left[A(u)\exp\left(-i\frac{2\pi}{\lambda_0}u\sin\theta\right)\right]$$
$$\propto \operatorname{sinc}\left[\left(\frac{x}{\lambda_0 z_f}+\frac{\sin\theta}{\lambda_0}\right)l\right]. \quad (3)$$

This can be clearly observed in the simulation results for the magnetic field in Fig. 4(a), where the $x$ position of peak of the sinc function at the back focal plane is clearly dependent on the angle of incidence. These angles are indicated on each sinc plot. According to Eq. (3) the peak of the sinc function should be located at −2.2, −4.4, −6.6, and −8.7 mm [shown as a cross on top of each sinc in Fig. 4(a)] for $\theta = 5$, 10, 15, and 20 deg, respectively. These "crosses" are indeed very close to the peak of the results obtained using the full-wave simulation. As an aside, it is interesting to note that by exploiting the

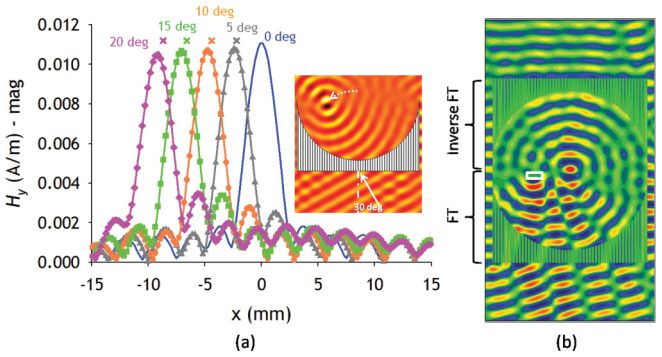


FIG. 4. (Color online) (a) Simulation results for the magnitude of the magnetic field distribution $H_y$ along the focal plane when the input signal is an obliquely incident plane wave: Normal incidence (blue curve), 5 deg incidence angle (gray triangles), 10 deg (orange circles), 15 deg (green squares), and 20 deg (pink diamonds). Top crosses (x) indicate the position of the sinc function according to theoretical Fourier transform. Inset: Magnetic field distribution (snap shot in time) in the $x$-$z$ plane when the incident angle is 30 deg. (b) Schematic of the principle of operation of two $\varepsilon$-near-zero metamaterial lens in cascaded performing spatial processing: Two plane waves with different angles of incidence illuminate the system; an absorbing material (boundaries highlighted in white) is placed at the focal point of one of them; at the output of the second lens, only one plane wave is remaining.

reciprocity, this feature can be used for mechanical beam steering in antennas applications: The direction of the beam emerging from the flat face of the lens would depend on the position of a primary source, when the source is moved along the $x$ axis in the back focal plane.

If the incoming wave is composed of two obliquely incident plane waves, we will expect to see two sinc functions whose peaks are displaced along the $x$ axis in the back focal plane of the lens according to the two angles of the incidence. By blocking one of these sinc functions in the back focal plane of the lens using a "filter" in that plane, and then utilizing another identical lens to inverse Fourier transform the remaining sinc function, we should obtain one of the two plane wave at the output of the second lens. This process can be viewed as an example of optical signal processing using such an ENZ lens. This can arguably be generalized, allowing us to manipulate the Fourier transform in the focal plane of such ENZ lens, and observe how this affects the "processed" image at the output. This strategy is represented in Fig. 4(b) where an illumination composed of a normally and an obliquely incident plane wave is considered. At the focal point corresponding to the obliquely incoming plane wave, an absorbing material is placed, leaving clearly just the normal incidence plane wave at the output.

Finally, as a byproduct of the properties of Fourier optics, "effective" negative refraction can be envisaged by placing two such ENZ lenses in cascade. This is illustrated in Fig. 5, where the Fourier transform of an obliquely incoming plane wave is formed on the back focal plane of the first ENZ lens and, afterwards, the inverse Fourier transform is performed by a second identical ENZ lens whose front focal plane coincides with the back focal plane of the first lens, effectively making a $4f$ system.[13] Effectively these two transformations in cascade produce a bend of the plane wave analogous to

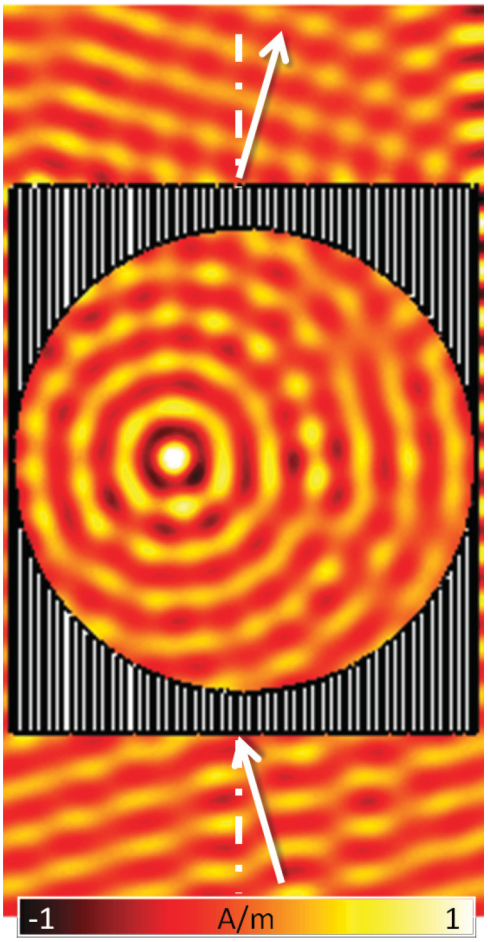


FIG. 5. (Color online) Effective negative refraction analogy by two $\varepsilon$-near-zero metamaterial lenses in cascade. Note that due to the finiteness of the lenses, the field pattern is distorted at the edges.

an effective negative refraction.[26] This approach to effective negative refraction may potentially be lossless, and thus, much more robust than the double-negative metamaterials. However, here we do not have subwavelength focusing, because this is not due to the negative index of refraction and moreover the focal plane is not in the near zone of the ENZ lens. One could then arguably suggest that this "effective" negative refraction may also be attainable with conventional glass-based lenses, which are diffraction limited as our ENZ lens is. However, these conventional lenses may be unmatched to free space, and thus, insertion losses may be unavoidable. The ENZ-based lenses suggested in the present work may, however, be matched with the free space, as mentioned above.

In summary, Fourier transformation has been numerically demonstrated with an array of waveguides near cutoff imitating an ENZ metamaterial lens. The results have been compared against theoretically expected Fourier transform, and also with the simulation results for the case of an isotropic homogeneous zero-refractive-index lens, showing good agreement. Owing to the narrow bandwidth of this waveguide system due to the ultranarrow width of the waveguides, frequencies different from the design frequency are filtered out, and thus improvement in the signal-to-noise level at the design frequency is expected. The approach shown here is a designable strategy for ENZ lenses at radio-to-THz frequencies attainable via conventional fabrication technologies already available for standard rectangular waveguides and may be extended to the THz or even optical regimes, due to the possibility of using natural ENZ electromagnetic responses.

The authors acknowledge fruitful discussion with Mário Silveirinha from the Department of Electrical Engineering—Instituto de Telecomunicações, University of Coimbra, Portugal. Effort sponsored by the Army Research Laboratory and the Air Force Office of Scientific Research, Air Force Material Command, USAF, under Grant No. FA8655-10-1-3078, and by the Spanish Government under contract Consolider "Engineering Metamaterials" CSD2008-00066. M.N.-C. acknowledges support from UPNA Mobility Grant 2010.

*m.navarro@imperial.ac.uk
†miguel.beruete@unavarra.es
‡mario@unavarra.es
§engheta@ee.upenn.edu

[1] R. W. Ziolkowski, Phys. Rev. E **70**, 046608 (2004).
[2] N. Engheta, Science **317**, 1698 (2007).
[3] N. Engheta, Phys. World **23**, 31 (2010).
[4] M. G. Silveirinha and N. Engheta, Phys. Rev. Lett. **97**, 157403 (2006).
[5] A. Alù, M. G. Silveirinha, A. Salandrino, and N. Engheta, Phys. Rev. B **75**, 155410 (2007).
[6] M. G. Silveirinha and N. Engheta, Phys. Rev. B **76**, 245109 (2007).
[7] L. Landau and E. M. Lifschitz, *Electrodynamics of Continuous Media* (Elsevier, New York, 1984).
[8] B. Edwards, A. Alù, M. E. Young, M. Silveirinha, and N. Engheta, Phys. Rev. Lett. **100**, 033903 (2008).
[9] M. G. Silveirinha and N. Engheta, Phys. Rev. Lett. **102**, 103902 (2009).
[10] M. Navarro-Cía, M. Beruete, I. Campillo, and M. Sorolla, Phys. Rev. B **83**, 115112 (2011).
[11] A. Alù and N. Engheta, Phys. Rev. B **78**, 045102 (2008).
[12] A. Alù and N. Engheta, Phys. Rev. Lett. **102**, 233901 (2009).
[13] J. W. Goodman, *Introduction to Fourier Optics* (Roberts & Company, Greenwood Village, 2004).
[14] M. Born and E. Wolf, *Principles of Optics: Electromagnetic Theory of Propagation, Interference and Diffraction of Light* (Cambridge University Press, Cambridge, 1999).
[15] R. H. Clarke and J. Brown, *Diffraction Theory and Antennas* (Ellis Horwood Ltd., Chichester, 1980).
[16] CST Studio Suite 2011, www.cst.com.
[17] L. Solymar and E. Shamonina, *Waves in Metamaterials* (Oxford University Press, Oxford, 2009).
[18] W. Rotman, IEEE Trans. Antennas Propag. **10**, 82 (1962).
[19] A. Alù, M. G. Silveirinha, and N. Engheta, Phys. Rev. E **78**, 016604 (2008).
[20] M. Silveirinha and N. Engheta, Phys. Rev. B **75**, 075119 (2007).

[21]W. E. Kock, Proc. IEEE **34**, 828 (1946).
[22]A. R. Dion and L. J. Ricardi, Proc. IEEE **59**, 252 (1971).
[23]M. Beruete, M. Navarro-Cía, M. Sorolla, and I. Campillo, Opt. Express **16**, 9677 (2008).
[24]M. Navarro-Cía, M. Beruete, M. Sorolla, and I. Campillo, Appl. Phys. Lett. **94**, 144107 (2009).
[25]M. Navarro-Cía, M. Beruete, I. Campillo, and M. Sorolla Ayza, IEEE Trans. Antennas Propag. **59**, 2141 (2009).
[26]V. G. Veselago, Sov. Phys. Usp. **10**, 509 (1968).